Characterization of the low energy conformations and differential reactivities of D-glucose and D-mannose based oxepines

Journal:	*Organic & Biomolecular Chemistry*
Manuscript ID	OB-ART-09-2021-001900.R2
Article Type:	Paper
Date Submitted by the Author:	20-Nov-2021
Complete List of Authors:	Griesbach, Caleb; University of Connecticut, Department of Chemistry Peczuh, Mark; University of Connecticut, Department of Chemistry

ARTICLE

Characterization of the low energy conformations and differential reactivities of D-glucose and D-mannose based oxepines

Caleb E. Griesbach [a] and Mark W. Peczuh [a]*

Carbohydrate-based oxepines are valuable intermediates for the synthesis of septanose carbohydrates. Here we report the characterization of the preferred conformations of D-glucose and D-mannose based oxepines **1** and **2** using computational chemistry and NMR spectroscopy. Monte Carlo conformational searches on **1** and **2** were performed, followed by DFT optimization and single-point energy calculations on the low energy conformations of each oxepine. Coupling constants were computed for all unique conformations at a B3LYP/6-31G(d,p)u+1s level of theory and weighted based on a Boltzmann distribution. These values were then compared to the experimental values collected using $^3J_{H,H}$ values collected from ^1H NMR spectra. Information from the MC/DFT approach was then used in a least squares method that correlated DFT calculated and observed $^3J_{H,H}$ coupling constants. The conformations of **1** and **2** are largely governed by a combination of the rigidifying enol ether element in combination with the reduction of unfavorable interactions. The vinylogous anomeric effect (VAE) emerged as a consequence, rather than a driver of conformations. Oxepine **1** showed greater reactivity in Ferrier rearrangement reactions relative to oxepine **2**, in line with its greater %VAE.

Introduction

Carbohydrate based oxepines are versatile starting materials for the synthesis of septanose carbohydrates. Reported methods for the preparation of these seven-membered ring ethers utilize ring closing metathesis,[1–4] cycloisomerization,[5,6] ring expansion,[7–10] or reductive elimination reactions[11] in the key step of their syntheses. The class of carbohydrate based oxepines under investigation here – specifically the 1,6-anhydro-2-deoxyhept-1-enitols **1** and **2** (Fig. 1) – are cyclic enol ethers. In many respects they are ring expanded homologs of 1,5-anhydro-2-deoxyhex-1-enitols (glycals). Both glycals and oxepines (i.e., D-xylose based oxepine **3**) can be converted to their corresponding 1,2-anhydrosugars, for example, and subsequently attacked by nucleophiles to form glycosidic bonds.[12–14,15] The allylic units in per-*O*-acetyl oxepines **1** and **2**, derived from D-glucose and D-mannose, are also poised for rearrangement via Ferrier (or Ferrier-like) reactions.[16] We reasoned that it was useful, therefore, to characterize the low energy solution conformations of **1** and **2** as we prepared to explore their reactivity. Motivation for the current study arose from numerous reports where the ground state conformations of glycals were linked with the reactivity and selectivity of transformations in which they participated.[13,17–21] A conformational analysis on the oxepines would also lay the
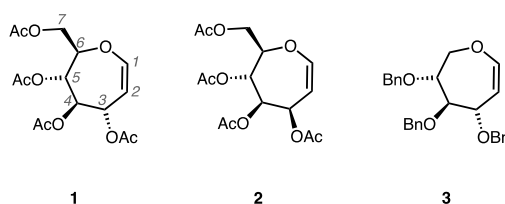

Figure 1. Carbohydrate based oxepines: per-*O*-acetyl D-glucose oxepine **1**, per-*O*-acetyl D-mannose oxepine **2**, and tri-O-benzyl D-xylose oxepine **3**.

groundwork toward understanding structural features that drive the conformation of the related seven-membered ring oxocarbenium ions.[22]

Conformational analysis of seven-membered ring systems can be loosely categorized into two broad classes, based on the types of compounds investigated. On one hand, there are studies on compounds like cycloheptane, oxepane, etc. that lack extensive functionality or stereochemistry.[23–25] On the other hand, there are studies on septanosides and related compounds that contain numerous functional groups and stereogenic centers.[1,3,26–28,29] In both classes of compounds, conformer populations primarily separate into equilibrating chair/twist-chair (*C/TC*) and boat/twist-boat (*B/TB*) manifolds (Fig. 2A) where the *C/TC* conformers are routinely of the lowest energy. When the compound contains a rigidifying functional group, as is the case for cycloheptene and oxepines, higher energy half-chair/twist-half (*H/TH*) conformers can also be observed (Fig. 2B).[3,23,30] Descriptions of the pathways for interconversion of conformers between the different equilibrating manifolds is possible using the Cremer-Pople formalism, but is cumbersome because of the extra parameters associated with seven-membered rings.[31,32] Regardless, the

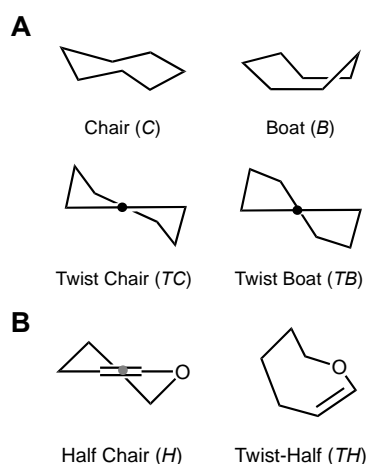a. *Department of Chemistry, University of Connecticut, 55 N. Eagleville Road, U3060, Storrs, CT 06269-3060, USA.*

Figure 2. A Conformations taken up by seven-membered rings: Chair, Boat, Twist Chair, and Twist Boat. **B** Conformations taken up by seven-membered rings containing a rigidifying unit like the alkene moiety of oxepines: Half Chair and Twist-Half. Note: The dot in the structures connotes the synclinal position.

population of low energy conformations in the highly functionalized systems is driven primarily by minimizing steric interactions and placing the hydroxymethyl substituent in an isoclinal position. Groups in the isoclinal position – the center of pseudosymmetry of the ring – are formally neither axial nor equatorial and do not suffer steric penalties (i.e. diaxial interactions).

Reports on the conformational analysis of glycals provided valuable context on the drivers of conformational preferences for oxepines. Glycals in the D-configuration primarily exist in two different half-chair (H) conformations, the $^4H_5$ and $^5H_4$, (Fig. 3A) with the former being dominant.[16] The energetic preference for the $^4H_5$ conformer is governed mostly by its ability to minimize steric interactions involving the C5 hydroxymethyl group when it is in an equatorial position. Another factor driving the energetics is the vinylogous anomeric effect (VAE).[33] The VAE is hyperconjugative delocalization of the endocyclic oxygen electrons into the σ* antibonding orbital (n→π→σ*) between C3 and a heteroatom with an electronegative group (Fig. 4). This stereoelectronic effect depends on the relative geometry of bonds and thus favors the quasi-axial orientation of the allylic substituent so as to align the σ* orbital with the π-electrons.[34] In the case of tri-O-acetyl-D-allal **5**, the two factors work in concert with the $^4H_5$ conformer (94% populated) where the acetate protected hydroxymethyl group is equatorial and the C3 acetoxy group is quasi-axial. For tri-O-acetyl-D-glucal **4**, the two effects work against each other. That is, the $^4H_5$ conformer has the C5 group equatorial but the $^5H_4$ has the C3 acetoxy group in a quasi-axial orientation. The result is that the two conformers are closer to 50:50, with the $^4H_5$ slightly preferred at 60%.[35,36] Conformational preferences can manifest themselves as differential reactivity. Under identical conditions, for example, the Ferrier rearrangement of 4,6-di-O-acetyl-3-(2-mercaptopyridine)-D-glucal **6** was three times slower than with its C3 epimer, 4,6-di-O-acetyl-3-(2-mercaptopyridine)-D-allal **7**.[37] The difference in reaction time can be linked to the conformational landscape of glycals **4** and **5** because the high population of the $^4H_5$ conformer for **5** (and presumably **7** as
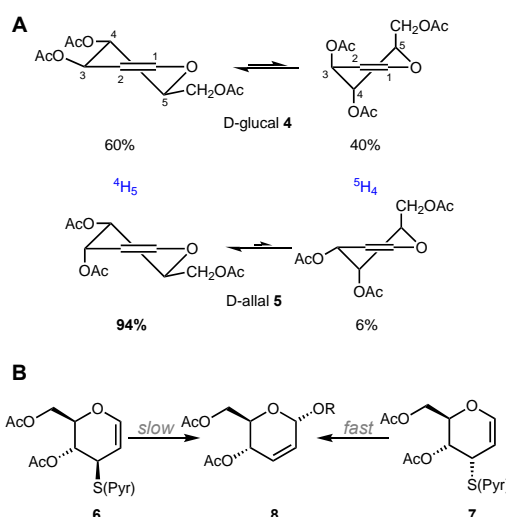

Figure 3. A Conformational equilibria of D-glucal **4** and D-allal **5**. **B** Ferrier rearrangements of **6** and **7** to for a 2,3-unsaturated O-glycoside **8**.
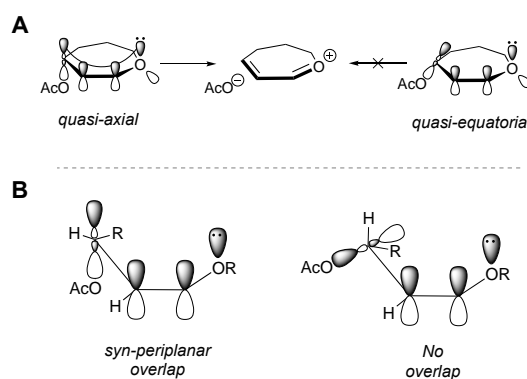

Figure 4. A Left – projection of an oxepine with a quasi-axial acetoxy group that allows overlap of the σ* with the n_o and π electrons facilitating ejection to form oxocarbenium; Right – projection showing a quasi-equatorial acetoxy with hindered overlap. **B** Left - generic case of the VAE which requires syn-periplanar overlap with the π elections; Right – a generic system showing no overlap between orbitals.

well) is poised for ejection of the C3 mercaptopyridine en route to an oxocarbenium ion and ultimately product **8**.

X-ray crystallographic data on 1,6-anhydro-3,4,5-tri-O-benzyl-2-deoxy-D-xylosept-1-enitol **3** (Fig. 1) showed that this compound adopted a $^6H_4$ conformation reminiscent of glycals.[15] It represents the only data we could find regarding conformations of the cyclic enol ether class of oxepines. The applicability to the present study is limited, though, because it was a solid-state conformation that may have been influenced by crystal packing forces and because the benzyl protecting groups are different electronically compared to the acetyl groups of **1** and **2**. Notably, the C3 benzyloxy group did not take up a quasi-axial disposition when **3** was in the $^6H_4$ conformation. At the outset, we expected to find that per-O-acetyl carbohydrate based oxepine conformations would be governed by the need to balance destabilizing trans-annular steric interactions of groups at the C6 position with the favorability of C3 electronegative groups that optimize the VAE. To this end, our goals for the study were to describe the low energy

conformations of **1** and **2** through a combination of computational chemistry matched with $^3J_{H,H}$ coupling constant analysis from ^1H NMR spectra. These data would enable the characterization of interactions that governed the distribution of conformers with a particularly focus on VAE. A clearer picture of the conformational preferences of **1** and **2** could then be used to rationalize results from Ferrier rearrangement reactions involving these oxepines.

Experimental Methods

1. Computational Methods: Monte Carlo Conformational Search, Optimization, and DFT Calculation of $^3J_{H,H}$ Coupling Constants

Structures of **1** and **2** were loaded into the Schrödinger Maestro interface. A Monte Carlo (MC) conformational search was performed in MacroModel[38] starting with the ring atoms in a co-planar (flat) configuration. Using the standard parameters, the ring was then opened, all torsion angles were randomly sampled, and then the ring was re-cycled. This resulting structure was minimized using the OPLSe force field in vacuo at 298 K. The minimized structure was then compared to the others using a RMSD statistic and kept if deemed to be unique. Conformers within an energy threshold of 5-500 kcal/mol and exceeding a RMSD of 0.5 Å were saved. Calculation of the RMSD value was done only for heavy atoms. This process was then repeated for at most 1000 steps or the algorithm converged to an energy minimum. Single-point energy calculations were done for all unique conformers generated in the MC search using a B3LYP/6-31G(d,p) level of theory.[39–41] Those within 20 kcal/mol of the global minimum and outside of an RMSD of 0.5 Å were passed along and optimized at the same level of theory. Conformers within 7 kcal/mol were again optimized using a finer grid and higher numerical precision. Again, these conformers were checked for uniqueness by a RMSD statistic.

Spin-spin coupling constants were calculated at a B3LYP/6-31G(d,p)u+1s level of theory for conformers within 7 kcal/mol of the global minimum. Single-point energy calculations were again carried out on the conformers using a conductor-like polarizable continuum model (CPCM). The energies calculated were used to create a Boltzmann distribution of conformers. Calculated coupling constants were combined based on the Boltzmann weights and scaled by a factor of 0.9155 detailed by Bally and Rablen.[42]

2. Collection of $^3J_{H,H}$ Coupling Constants by ^1H NMR

Oxepines **1** and **2** were synthesized from tetra-*O*-benzyl D-glucose and tetra-*O*-benzyl D-mannose as previously described by us.[11] Samples of each (650-700 μL of a ~10 mM solution) were prepared in a wide range of solvents along the dielectric continuum including: d1-chloroform, d3-acetonitrile, d6-benzene, d6-acetone, and d2-dichloromethane Spectra were collected on either a Bruker Avance 500 MHz (FIDRES = 0.31 Hz) or a Bruker Avance III 400 MHz instrument (FIDRES = 0.44 Hz). FIDRES is an expression of the resolution of the ^1H NMR spectra and sets the limits on the error associated with $^3J_{H,H}$ coupling constant values. Other NMR parameters are tabulated in the ESI. A preliminary 1D ^1H NMR experiment was then performed

as a quality check. If water was found in the sample, an activated 4 Å molecular sieve pellet or $CaCl_2$ pellet was added. This worked for almost every solvent except for acetone and acetonitrile which continued to contain trace amounts of water. Then standard 1D ^1H spectra were used to extract homonuclear $^3J_{H,H}$ coupling constants.

3. Reactions of oxepines 1 and 2

*Ferrier reaction in HFIP to form septanoside **7***. This procedure based on the one reported by Di Salvo et al.[43] Oxepine **1** (26.9 mg, 0.0781 mmol) was dried by azeotropic distillation in toluene (3 x 1.0 mL), then dissolved in HFIP (2.0 mL) and placed in a bath at 60 – 65 °C. The mixture was refluxed for 16 h under nitrogen atmosphere and then the contents were allowed to cool to room temperature. The solvent was removed under reduced pressure, the residue was redissolved in EtOAc (1.0 mL) and concentrated again to ensure removal of HFIP. Purification of the reaction mixture via column chromatography (40% EtOAc/Hex) provided a white solid (13.8 mg, 39%). %). mp 97.5-99.7 °C; R_f 0.64 (40% EtOAc/Hex); ^1H NMR (400 MHz, CDCl$_3$) δ 6.05 (ddd, J = 12.17, 5.83, 1.63 Hz, 1H, H3), 5.78 (dd, J = 12.17 Hz, 2.14 Hz, 1H, H2), 5.67 (br s, 1H, H1), 5.30-5.23 (m, 2H, H4/5), 4.70 (sept, 5.88 Hz, 1H, CH-(CF$_3$)$_2$), 4.30 (ddd, J = 8.75, 3.91, 2.81 Hz, 1H, H6), 4.28 (dd, J = 12.65, 2.53 Hz, 1H, H7), 4.22 (dd, J = 12.43, 4.51 Hz, 1H, H7') 2.12 (s, CH$_3$-C=O), 2.10 (s, 3H, CH$_3$-C=O), 2.08 (s, 3H, CH$_3$-C=O); ^{13}C NMR (100 MHz, CDCl$_3$) δ 170.78 (C=O), 169.75 (C=O), 169.18 (C=O), 129.28 (C2), 128.55 (C3), 99.45 (C1), 72.19 (C4/5/6), 71.19 (m, CH-(CF$_3$)$_2$), 70.18 (C4/5/6), 70.16 (C4/5/6), 63.04 (C7), 20.89 (CH$_3$-C=O), 20.85 (CH$_3$-C=O), 20.80 ((CH$_3$-C=O); ^{19}F NMR (376 MHz, CDCl$_3$, C$_6$F$_6$) δ -75.90 (dq, J = 18.05, 9.20, 5.79 Hz, CF$_3$), -76.38 (dq, J = 18.05, 9.20, 6.47 Hz, CF$_3$); TOF HRMS (ESI) *m/z* calcd for C$_{16}$H$_{18}$F$_6$O$_8$ (M+Na)$^+$ 475.0798, found 475.0724.

NiCl$_2$ mediated Ferrier isomerization. This is a representative procedure using oxepine **1** as starting material. It is based on the procedure reported by Inaba et al.[44] Oxepine **1** (26.5 mg, 0.0770 mmol) was dried by azeotropic distillation in toluene (3 x 1.0 mL), then acetic anhydride (0.90 mL, 9.5 mmol) and nickel(II) chloride hexahydrate (18.9 mg, 0.0795 mmol) were added to the reaction flask. The solution was heated for 1 h at 120 °C, filtered through celite, and rinsed with dichloromethane (100 mL). The filtrate was washed with saturated aqueous NaHCO$_3$ (1 x 50 mL), water (1 x 50 mL), and brine (1 x 50 mL). The organic layer was separated and dried with Na$_2$SO$_4$ and then the solvent was removed under vacuum to give a yellow syrup. This residue was purified via column chromatography to yield **10** as colorless syrup as a 7:1 mixture of anomers (7.0 mg, 26 %). R_f 0.42 (70 % Et$_2$O/Hex); major isomer (α): ^1H NMR (300 MHz, CDCl$_3$) δ 6.55 (dd, J = 1.49 Hz, 1H, H1), 6.04 (ddd, J = 11.97, 6.22, 1.63 Hz, 1H, H3), 5.68 (dd, J = 11.99, 2.12 Hz, 1H, H2), 5.24 (dd, J = 6.20, 3.83 Hz, 1H, H4), 5.14 (dd, J = 9.32, 3.80 Hz, 1H, H5), 4.30 (ddd, J = 9.32, 6.78, 2.63 Hz, 1H, H6), 4.19 (dd, J = 11.83, 6.84 Hz, 1H, H7), 4.09 (dd, J = 11.87, 2.75 Hz, 1H, H7), 2.12 (s, 3H, CH$_3$-C=O), 2.08 (s, 3H, CH$_3$-C=O), 2.07 (s, 3H, CH$_3$-C=O), 2.06 (s, 3H, CH$_3$-C=O) ^{13}C NMR (75 MHz, CDCl$_3$) δ 170.74 (C=O), 169.97 (C=O), 169.38 (C=O), 169.26 (C=O), 130.56 (C2), 128.41 (C3), 92.87 (C1), 73.20 (C4), 71.05 (C6), 70.30 (C5), 63.98
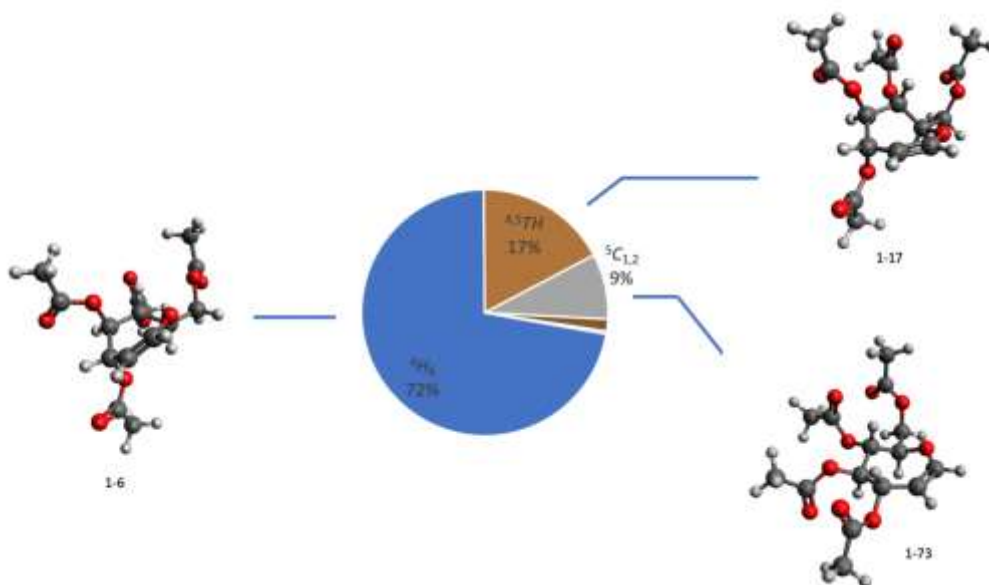
Figure 5. Boltzmann Distribution of **1** in chloroform ($\varepsilon = 4.81$). $^4H_6$ (blue) 72%; ^{45}TH (brown) 17%; $^5C_{1,2}$ (gray) 9%; ^{56}TH (dark brown) 2%. Conformers 1-6 ($^4H_6$), 1-17 (^{45}TH), and 1-73 ($^5C_{1,2}$) were the lowest energy conformer of each class.
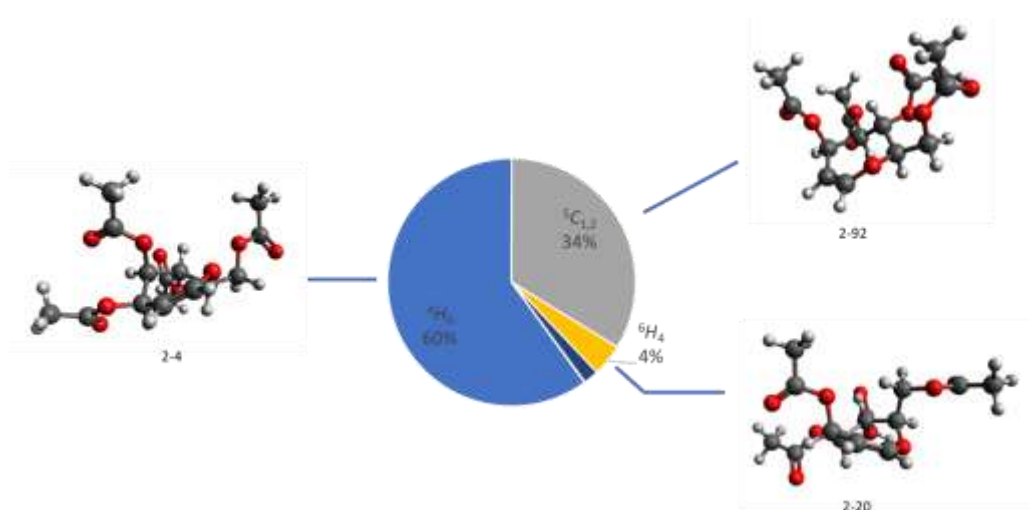

Figure 6. Boltzmann Distribution of **2** in chloroform ($\varepsilon = 4.81$). $^4H_6$ (blue) 60%; $^5C_{1,2}$ (gray) 34%; $^6H_4$ (gold) 4%; $^{1,2}C_5$ (dark blue) 2%. Conformers 2-4 ($^4H_6$), 2-92 ($^5C_{1,2}$), and 2-20 ($^6H_4$) were the lowest energy conformer of each class.

(C7), 21.22 (CH$_3$-C=O), 20.93 (CH$_3$-C=O), 20.91 (CH$_3$-C=O), 20.86 (CH$_3$-C=O); minor isomer (β): ^{1}H NMR (300 MHz, CDCl3) δ 6.20 (dd, 1H, H1), 5.94 (ddd, J = 11.85, 2.36, 1.97, 1H, H2), 5.79 (ddd, J = 11.76, 3.99, 1.95, 1H, H3), 5.65-5.58 (m, 1H, H4), 5.18-5.10 (m, 1H, H5), 4.41-4.34 (m, 1H, HC7), 4.19 (dd, J = 11.83, 6.84 Hz, 1H, H7'), 4.19-4.14 (m, 1H, H6), 2.13 (s, 3H, CH$_3$-C=O), 2.07 (s, 3H, CH$_3$-C=O), 2.06 (s, 3H, CH$_3$-C=O), 2.05 (s, 3H, CH$_3$-C=O); ^{13}C NMR (75 MHz, CDCl$_3$) δ 170.89 (C=O), 169.90 (C=O), 169.38 (C=O), 169.26 (C=O), 132.03 (C2), 130.79 (C3), 93.25 (C1), 77.56 (C6), 71.47 (C4), 69.87 (C5), 63.83 (C7)s, 21.12 (CH$_3$-C=O), 20.93 (CH$_3$-C=O), 20.91 (CH$_3$-C=O), 20.86 (CH$_3$-C=O); TOF HRMS (ESI) m/z calcd for C$_{15}$H$_{20}$O$_9$ (M+NH$_4$)$^+$ 362.1446, found 362.1457.

Results

1. Characterization of the low-energy conformations of 1 and 2 by Monte Carlo and DFT Optimizations

The MC conformational search conducted on compounds **1** and **2** uncovered 2,749 and 3,287 different conformers, respectively. After careful elimination of redundant conformers by iteratively decreasing the energy cut-off and increasing the calculation complexity (basis set and functional), 69 conformers for **1** and 63 conformers for **2** were found within 7 kcal/mol of the respective minimum energy conformers. Table 1 summarizes the characteristics of the conformational profiles of

1 and **2** in terms of number of conformers and Boltzmann contribution of individual bins and their relative energies. A

Table 1. Characteristics of the conformations of oxepines **1** and **2**.

Oxepine	Conformer Bin	No. of Conformers	χ%[a]	$\bar{E}_{rel}$ (kcal/mol)[b]
	$^4H_6$	17	71.7%	2.09
1	$^{4,5}TH$	15	17.3%	3.09
	$^5C_{1,2}$	11	8.5%	3.11
	$^4H_6$	26	60.0%	2.98
2	$^5C_{1,2}$	13	33.7%	3.00
	$^6H_4$	10	4.2%	4.24

[a] χ% is the cumulative Boltzmann population for each conformer bin; [b] $\bar{E}_{rel}$ is the average relative energy of the conformers in a bin in comparison to the to the global minimum.

table with more details on the conformers is in the ESI (Table S1). Conformers for each compound were then coded to reflect their identity and position in the original list (e.g., 1-6 is the sixth conformer found for compound **1**). Each conformer was also grouped by visual inspection into specific chair (*C*), half-chair (*H*), or twist-half (*TH*) conformer bins based only on the ring conformation using Stoddart's nomenclature for carbohydrate ring conformations.[45] In practical terms, this meant that compounds with the same ring conformation but different C6-C7 rotamers or acetate configurations were put into the same bin. New single-point energy calculations were then carried out on all conformers that now included the CPCM solvation model matched to chloroform. Of these, 53 conformers of **1** and 45 conformers of **2** were found to be within 5 kcal/mol of the global minimums and were used for the calculation of spin-spin coupling constants (SSCC).

The MC/DFT process partitioned compounds **1** and **2** into bins of conformers based on the shape of the seven-membered ring. With regard to compound **1**, the $^4H_6$, $^{4,5}TH$, and $^5C_{12}$ conformations were preeminent, accounting for approximately 97% of the Boltzmann distribution (Fig. 5). Among them, the $^4H_6$ half chair dominated, accounting for 72% of the overall Boltzmann distribution at room temperature. This conformer has a molecular plane containing the ring O, C1, C2, C3, and C5. The four-atom unit (ring O-C3) encompasses the enol ether unit, with C4 and C6 above and below that plane. Flanked by C4 and C6, C5 sits coplanar with the atoms of the enol ether. The exocyclic acetoxymethyl group at C6 is quasi-equatorial in this conformation and the C3 and C4 acetoxy groups are quasi-axial. The $^{4,5}TH$ and $^5C_{1,2}$ conformations make up the remainder of the Boltzmann distribution, with 17% and 8% contributions, respectively. The $^{4,5}TH$ conformer is defined by a five-atom plane containing C6, O, C1, C2, and C3, with C4 and C5 tilted above the molecular plane. In this conformation, the disposition of the C3 and C4 acetoxy groups, and the C6 acetoxymethyl group is the same as in the $^4H_6$ conformer. The $^5C_{1,2}$ conformation differs from $^4H_6$ and $^{4,5}TH$ because the enol ether is not part of the molecular plane. Instead, the plane is composed of two pairs of atoms: C6 and the ring oxygen, and C3 and C4, with the double bond of the enol ether (C1 and C2) below the molecular plane and C5 above it. Here all the groups

attached to C3-C6 are quasi-equatorial. Of the major conformer bins, the $^4H_6$ and $^{4,5}TH$ display quasi-axial C3 acetoxy groups (C1-C2-C3-O dihedral ≈ 90°), accounting for 89% of all conformers; this configuration is consistent with the VAE.

Inspection of the MC/DFT results on **2** showed that the $^4H_6$, $^5C_{1,2}$, and $^6H_4$ were the most prevalent conformations, accounting together for about 98% of the Boltzmann distribution (Fig. 6). Analogous to **1**, $^4H_6$ was the most dominant conformer of **2** at 60%, and the $^5C_{1,2}$ was second at 34%. Both of these conformers carry the same geometrical idiosyncrasies of the ring as described for compound **1**. The $^6H_4$ conformation accounted for 4% of the population for **2**. This conformer is defined by the same plane as the $^4H_6$, but the locations of C4 and C6 switch, with C6 above the plane and C4 below it. Since **2** and **1** are epimeric at C3, the $^4H_6$ conformation for **2** does not exhibit a quasi-axial acetoxy group, but the $^5C_{1,2}$ and $^6H_4$ do. Thus, only about 38% of the population distribution adopts a geometry in line with the VAE.

Of the exocyclic substituents, the acetoxymethyl group is the most influential toward overall energy. The C6-C7 rotamer can occupy three different conformations; gg, gt, and tg (Fig. S2).[46] Both **1** and **2** have similar rotamer population distributions with a 64:35:1 gg:gt:tg ratio for **1** and a 66:27:7 ratio for **2**, as predicted by DFT. The preference for gg and gt conformations can be attributed to the gauche effect with an additional stabilization for the gg conformation by hyperconjugation between $\sigma_{C6-H6} \rightarrow \sigma^*_{C7-O7}$.[47] Based on its size, the acetoxymethyl (CH$_2$OH A-value = 1.76) group also influences ring puckering more than the other acetates (OAc A-value = 0.68).[48] Its increased bulkiness causes the ring to pucker so that the C7 substituent prefers an equatorial position. For **1**, the $^4H_6$, $^{4,5}TH$, and $^5C_{1,2}$ conformers all meet this equatorial requirement. Likewise, the $^4H_6$ and $^5C_{1,2}$ conformers of **2** meet it. The exception is the $^6H_4$ conformation of **2**, where the acetoxymethyl group is quasi-axial. Energetically favorable interactions can be mediated by the acetoxymethyl group as well. Because of their proximity to each other, the C5 and C7 acetate carbonyls of oxepine **1** align in an anti-periplanar fashion with each other in the lowest $^4H_6$ conformer (1-6); this alignment is presumably due to the complementarity between their partial charges. This C5-C7 acetate orientation occurs in seven of the 53 low energy conformers of **1**, 48% of the Boltzmann distribution, and seven of the 45 low energy conformers of **2**, 56% of the distribution. Additionally, the rotamer has to be in a gg or tg conformation to align carbonyls.

The associative interaction between anti-periplanar carbonyls observed for the C5 and C7 acetates was also observed for vicinal acetates at other positions along the backbone of the oxepines (i.e., C3-C4, C4-C5). Acetate ester groups by and large adopted the *Z* conformation where the carbonyl oxygen of the ester eclipsed the hydrogen of a given ring carbon (Fig. S1A).[45,48,49,50] We also observed that, in this conformation, one hydrogen of the methyl group on the acetyl unit would align itself so that it was eclipsing/co-planar with its carbonyl oxygen (Fig. S1B). When vicinal acetates were in a gauche conformation, their carbonyls orient themselves in a pseudo anti-periplanar fashion so that their partial charges

align. (Fig. S1C) This interaction does not occur in the $^4H_6$ (1-6) conformation except for the C5 and C7 acetates.
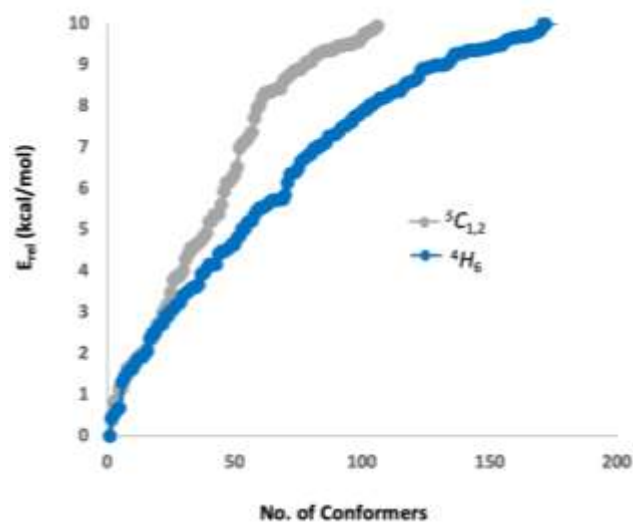

Figure 7. Cumulative frequency analysis of the two major conformations of **2**.

Pseudorotation from this conformation to the $^{4,5}TH$ (1-17) decreases the torsion angle between the C4 and C5 acetates to a staggered gauche orientation. In this position, the two acetates are able to align their carbonyls. The $^5C_{1,2}$ conformer of **1** (1-73) is primed for this type interaction because of the staggered gauche orientation of the substituents allowing for interaction between the C3-C4 and C5-C7 acetate carbonyls. In the identical $^5C_{1,2}$ conformer of **2** (2-92), the C3 acetate is in a quasi-axial orientation, thus only the C5-C7 acetate carbonyls align.

In an effort to get a better sense of the influence of the acetate orientations and C6-C7 rotamers on overall energy and simultaneously explain the discrepancy between the global minimum versus most highly populated conformers of **2**, a cumulative frequency analysis was conducted. Conformers 2-4 and 2-92—the lowest $^4H_6$ and $^5C_{1,2}$ conformations, respectively—were used as the starting points and inserted into a MC conformational search. In this routine, the ring geometry was fixed and the torsion angles of the exocyclic substituents were explored exclusively. The search was performed using the OPLSe force field matched to vacuum. RMSD calculations were only performed using atoms included in the acetate groups. Conformers with an RMSD > 0.5 Å were considered unique. All in all, this resulted in 931 unique $^5C_{1,2}$ conformations (starting from conformer 2-92) and 1429 $^4H_6$ conformations. The OPLSe forcefield energies were used since we were only interested in a qualitative analysis between the two classes. Because the MC search found more $^5C_{1,2}$ conformers, the relative energy increased at a higher rate than for the $^4H_6$ conformation (Fig. 7). This indicated that the energy gaps between conformers with different configurations of exocyclic groups were farther apart. This explains why we observed a $^5C_{1,2}$ global minimum but a dominant $^4H_6$ Boltzmann distribution for **2**: the shape of the energy well for the $^5C_{1,2}$ conformer is narrow and steep relative to the $^4H_6$ conformational well. Because the $^4H_6$ well is shallower, less energy is required to change exocyclic

conformations. Within 5 kcal/mol, then, there are more states the exocyclic substituents can adopt for $^4H_6$ conformers.

2. Characterization of oxepine conformers by comparing DFT-calculated and ^1H NMR-observed $^3J_{H,H}$ coupling constants

The $^3J_{H,H}$ coupling constants for all the ring protons on each of the 69 conformers of **1** and 63 conformers of **2** were calculated at the B3LYP/6-31G(d,p)u+1s[H] level of theory in vacuum. This level of theory was chosen because Bally and Rablen demonstrated that it is effective for the accurate calculation of inter-proton coupling constants in a variety of small, rigid molecules.[42] Coupling constants for each conformer of a given oxepine gathered by this method were scaled by a factor of 0.9155 and then weighted by its contribution to the Boltzmann distribution as described below. Results from this process gave the MC/DFT-calculated $^3J_{H,H}$ values listed in Table 2.

We then sought to compare the calculated $^3J_{H,H}$ values to experimental values extracted from ^1H NMR spectra collected in chloroform. One dimensional ^1H NMR spectra of **1** and **2** were collected at 500 MHz at room temperature. The chemical shifts were sufficiently disperse to allow determination of coupling constants directly from these spectra. Observed coupling constants were extracted using the multiplet tool in Topspin. Coupling constant values from both signals for two correlated protons were averaged to get the $^3J_{H,H}$ value shown in Table 2.

There is very good qualitative agreement between the calculated and experimental $^3J_{H,H}$ values for both **1** and **2**. In particular, the $^3J_{H,H}$ values between C2-C6, which house the key information about the conformation of the oxepine ring, are excellent. To express the agreement of these values quantitatively, RMSD values were calculated for **1** and **2**. For **1**, an RMSD of 0.91 Hz amongst all $^3J_{H,H}$ values (C1 through C7) of the molecule was calculated and a similar RMSD of 1.00 Hz was obtained for **2**. Removing the $^3J_{H,H}$ values involving C7 - the exocyclic acetoxymethyl group - from the RMSD calculation gave values of 1.03 Hz and 0.81 Hz for **1** and **2**, respectively. An earlier conformational analysis of methyl septanosides had difficulty predicting C6-C7 rotamer populations in solution. While the restricted RMSD calculation led to a lower value for **2**, there was an increase in error for **1**. This suggested that the source of error resides in the MC/DFT-predicted distribution of ring geometries for **1**, not the DFT calculation of coupling constants. As became clear later (vide infra), it may be that chair conformations account for too small of a subset in the DFT Boltzmann distribution (7-10%) for **1**. Other seven-membered ring systems with a rigidifying bond (i.e. amide, ester, alkene) prefer chair conformations and the increased RMSD error for **1** could be caused by an underprediction of that conformation.[3,23,27]

A least squares regression approach was taken to re-investigate the conformer populations by correlating the calculated $^3J_{H,H}$ coupling constants with the experimentally determined values for **1** and **2**. Only the most dominant conformers were considered for the regression. These were the $^4H_6$, $^5C_{1,2}$, and $^{4,5}TH$ for **1** and the $^4H_6$ and $^5C_{1,2}$ for **2**. Including the $^6H_4$ conformer – a minor contributor in the DFT calculated Boltzmann – in the least squares analysis led to negative

populations for compound **2**, so it was omitted. Solving the equations (See ESI for equations.) with coupling constants
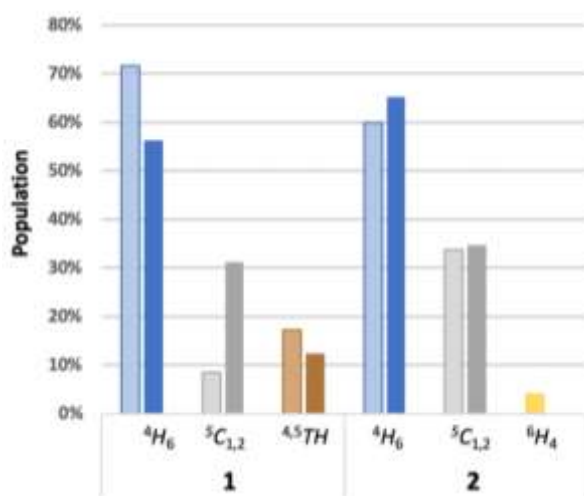

Figure 8. Populations of the most dominant conformations for **1** and **2** based on the MC/DFT (light) and least squares (solid) methods.

extracted from the ^{1}H NMR spectrum led to some reorganization of the conformer bins (Fig. 8). Nonetheless, the coefficient of determination (R^2) for the regression was 0.99 for nearly all datasets. For **1**, the population of the $^4H_6$ conformer deteriorated but it was still dominated the overall population. Ordering of the $^{4,5}TH$ and $^5C_{1,2}$ conformers, on the other hand, switched, where the $^5C_{1,2}$ was now favored; this result implies a shortcoming in the DFT method which may have biased the $^{4,5}TH$ conformer at the expense of the $^5C_{1,2}$. Another possibility is that the $^{4,5}TH$ is an intermediate conformer that resides between different conformations of **1**. The preference for the $^5C_{1,2}$ conformation is in line with previous conformational analyses of unsaturated seven-membered rings.[3,23,27] Conformer populations of **2** computed by the least squares method were largely aligned with the MC/DFT Boltzmann distributions. The minor contribution of the $^6H_4$ conformer to the MC/DFT Boltzmann distribution (4%) was redistributed nearly between the $^4H_6$ and $^5C_{1,2}$ conformers in the least squares method. The percentage of conformers of **1** exhibiting the VAE dipped from 89% to 69% when going from the MC/DFT to the least squares method. For **2**, the %VAE – the fraction of all conformers exhibiting the VAE – remained steady at around one-third of conformers (38% for MC/DFT and 35% for least squares). Pictured through the lens of the least squares method, the conformer populations of **1** and **2** are largely similar, so the differential in their %VAE arises from the difference in the absolute configuration at C3.

Since rigid molecules essentially adopt one major conformation, we reasoned that Bally and Rablen's DFT method[42] for the calculation of SSCC would also be accurate for individual conformers of a flexible molecule. We argue that $^3J_{H,H}$ values computed by this method using exemplars for each conformer, combined with the accuracy of the least squares regression, make these populations the best conformational profiles of **1** and **2**. That is, the MC/DFT method underpredicts

chair conformations causing some error represented in the RMSD value. This error is corrected in the least squares method

Table 2. Observed and calculated $^3J_{H,H}$ coupling constants of **1** and **2** in chloroform.

	1			**2**	
$^3J_{H,H}$	NMR-obs[b] (Hz)	DFT-calc (Hz)	$^3J_{H,H}$	NMR-obs[b] (Hz)	DFT-calc (Hz)
$^3J_{1,2}$	6.95	7.43	$^3J_{1,2}$	6.84	7.52
$^3J_{2,3}$	6.15	7.49	$^3J_{2,3}$	3.44	4.52
$^3J_{3,4}$	5.73	5.21	$^3J_{3,4}$	1.77	2.27
$^3J_{4,5}$	4.10	2.49	$^3J_{4,5}$	4.10	4.87
$^3J_{5,6}$	9.66	10.33	$^3J_{5,6}$	8.90	9.79
$^3J_{6,7}$	2.23	1.66	$^3J_{6,7}$	2.54	2.07
$^3J_{6,7'}$	5.15	4.86	$^3J_{6,7'}$	6.31	4.44
RMSD (all)[c]		0.91	RMSD (all)		1.00
RMSD (ring)		1.03	RMSD (ring)		0.81

[a] DFT computed $^3J_{H,H}$ values based on the Boltzmann distribution of conformers; [b] Approximate error of $^3J_{H,H}$ values based on the resolution of ^{1}H NMR spectra was 0.31-0.44 Hz; [c] RMSD (all) = all protons in carbohydrate moiety, RMSD (ring) = protons in ring system.

by approximating the populations to the DFT calculated coupling constants to those observed in the NMR spectra. With this method, the $^5C_{1,2}$ and $^{4,5}TH$ conformers reverse hierarchy in **1** and in **2** the hierarchy remains the same.

3. The effect of solvent dielectric on conformer populations

The effect of solvent dielectric on the populations of conformers for **1** and **2** was also investigated. Single-point energy calculations were carried out on all vacuum optimized conformers within 7 kcal/mol of the global minimum for **1** and **2** using the CPCM solvation model matched to other solvents in addition to chloroform (ε = 4.81). Solvents were chosen to be aprotic and encompass a wide range of dielectric constants. These included benzene (ε = 2.27), dichloromethane (ε = 8.96), acetone (ε = 20.7), and acetonitrile (ε = 37.5). Since polar solvents are better at stabilizing charged species, we expected to observe an increase in percent VAE (%VAE) due to the polarization of the ring O-C1-C2-C3 system when the C3 acetoxy group is quasi-axial. Increased VAE would result in an associated change in the distribution of conformer populations. This reasoning predicted an increase in $^4H_6$ and $^{4,5}TH$ populations for **1** and $^5C_{1,2}$ and $^6H_4$ populations for **2**. This was not the case, however. Instead, the $^4H_6$ conformer population increased with solvent polarity for both oxepines, although the shift was more pronounced for **1** than for **2**. (Fig. S3)

Recourse to the least squares method was then initiated to once again improve perspective on the conformer populations of **1** and **2** in the various solvents. A pre-requisite for the analysis was the acquisition of $^3J_{H,H}$ coupling constants by ^{1}H NMR spectra for each oxepine in the solvents (Table S5 and S6) mentioned. Just like the initial analysis in chloroform, RMSD calculations were performed for all vicinal protons and those incorporated in the ring moiety (Tables S5 and S6). For **1**, the RMSD values show good agreement for all solvents, ranging from 0.85-1.08 Hz and 0.93 – 1.06 Hz for **2**. The low RMSD values reflected the fidelity between the computed (MC/DFT) and

observed conformer populations. By and large, the least squares conformer populations of **1** and **2** were stable across
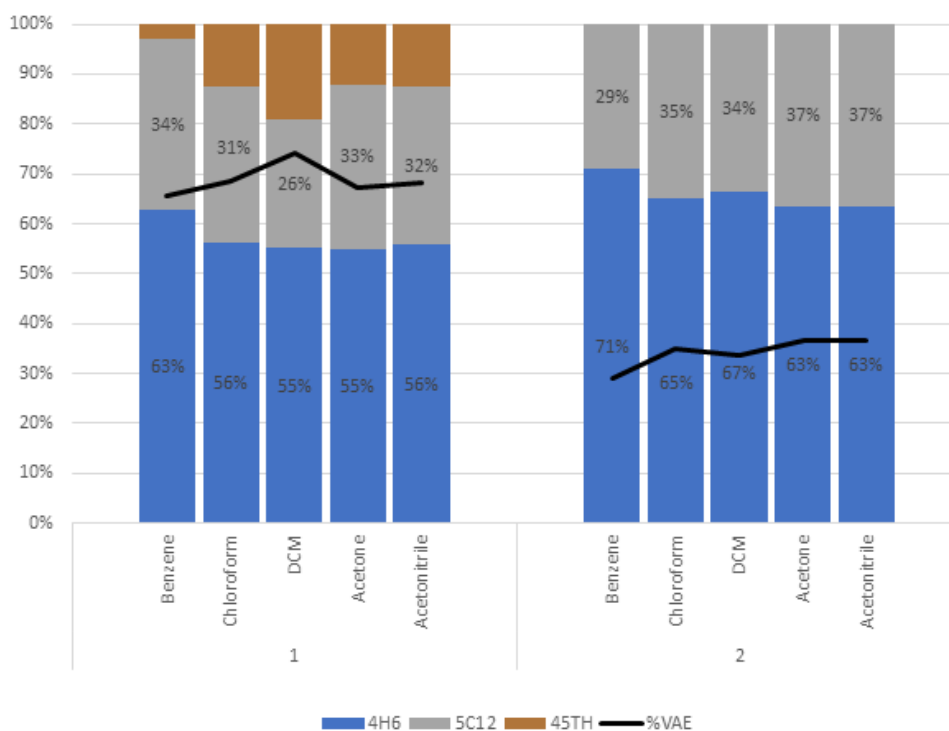

Figure 9. Populations of **1** and **2** in various solvents as determined by the least squares regression method.

the solvents investigated (Fig. 9). For **1**, increases in the $^5C_{1,2}$ population were paid through decreases in both the $^4H_6$ and $^{4,5}TH$ bins. For **2**, the population was simply stable across the solvents, hovering around a roughly 2:1 ratio of $^4H_6$ to $^5C_{1,2}$ conformer populations. A few important takeaways were collected through analysis of the conformer populations over the group of solvents. First, because the conformer populations were stable, the %VAE did not change drastically either. Second, it suggested that VAE is less a driver of conformations in highly functionalized oxepines like **1** and **2** and more likely an accessory consequence of them. Last, %VAE is significantly higher in the conformer population of D-glucose based oxepine **1** than it is for D-mannose based oxepine **2** (~69 to ~34%, respectively). Despite the similar energies of the different conformations, the impact of the difference %VAE between **1** and **2** were kept in mind as the reactivity of **1** and **2** were evaluated. Also, even though the least squares method calculated a decrease of %VAE for **1** compared to the MC/DFT method, the disparity of %VAE between **1** and **2** is still consistent between the two methods.

4. Differential reactivities of oxepines 1 and 2 under Ferrier conditions

The differences in the conformational profiles of oxepines **1** and **2**, like those of glucal **4** and allal **5**, suggested that there may be differences in their reactivity. We set about evaluating this notion using Ferrier reactions. Refluxing tri-*O*-acetyl-D-glucal in hexafluoroisopropyl alcohol (HFIP), for instance, was shown to facilitate Ferrier rearrangements to form 2,3-dehydro HFIP glycosides.[43] Under the reaction conditions (refluxing HFIP, 16h), oxepine **1** afforded HFIP 2,3-dehydro septanoside **9** in 39%

yield (Fig. 10). The product was of one anomeric configuration. The ^{13}C NMR for C1 was at 99.62 ppm and NOESY experiments showed a distinct correlation between H1 and H6. Together, these data showed that **9** was the β-anomer. We propose that it arose by equilibration to the more thermodynamically stable anomer under the reaction conditions. Since **1** and **2** prefer to adopt half-chair conformations, we infer that β-glycoside **9** will adopt a ^5H_O conformation, which benefits energetically from the anomeric effect. When oxepine **2** was subjected to the identical reaction conditions, only starting material was recovered from the reaction (64%). Alternative reaction conditions were explored with the intention of transforming **2** via a Ferrier rearrangement. Specifically, extending the reaction time to 50 h did not lead to observable reaction and, separately, addition of catalytic amounts of 10 mole percent *p*-tosic and triflic acid to the reaction were also unsuccessful in transforming oxepine **2**.
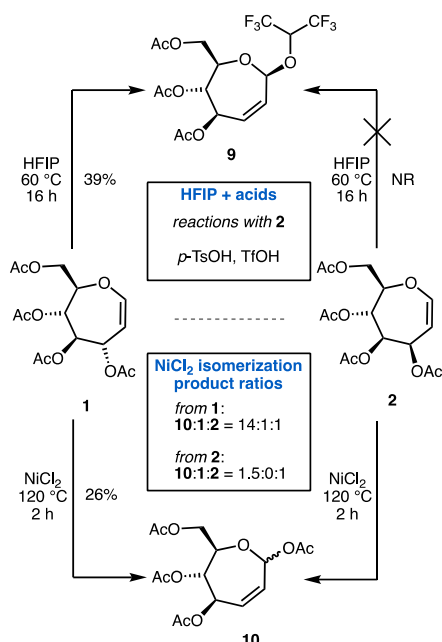
Figure 10. Ferrier reactions of oxepines **1** and **2**

A nickel-mediated Ferrier rearrangement presented a useful way to further characterize the differential reactivities of **1** and **2** under conditions used to epimerize glycals.[44,51] We expected to get information about the equilibrium mixture of products from the reaction. Under thermodynamic conditions, the major product (or products) would be dictated by their relative stabilities. For tri-*O*-acetyl D-glucal **4** and D-allal **5**, this was the 2,3-dehydro pyranoside (e.g., **8** in Fig. 3). Upon reaction, oxepine **1** yielded 1,4,5,7-tetra-*O*-acetyl-α/β-D-*arabino*-hept-2-enoseptanoside **10** as the major product, along with unreacted starting material and also **2**, the C3-epimeric oxepine. The ratio the products was 14:1:1 (**10**:**1**:**2**) based on ^{1}H NMR integration of the reaction mixture after work-up. When **2** was subjected to the same reaction conditions, only **10** and **2** were isolated (1.5:1 ratio by ^{1}H NMR integration). In Figure 11, details of ^{13}C NMR spectra showing signals corresponding to the allylic system of oxepines **1** and **2** and 2,3-dehydro septanoside **10** (as a mixture of anomers). The figure also shows the same spectral regions for the product mixtures of NiCl₂ isomerization reactions starting from **1** and **2**. The observation that both **1** and **2** were converted to 2,3-dehydro septanoside **10** as the major product indicated that the glycoside was the most thermodynamically stable species of the three. Further, the appearance of **2** in the reaction where **1** was the starting material indicated that the oxepine **2** was more stable than **1**. This interpretation is reinforced by the fact that **1** did not appear in reactions that began with **2**.

Discussion

The analysis here draws correlations between the conformational profiles of oxepines **1** and **2** and their reactivities in the Ferrier rearrangements but refrains from invoking causation. A complete rationale for the physical
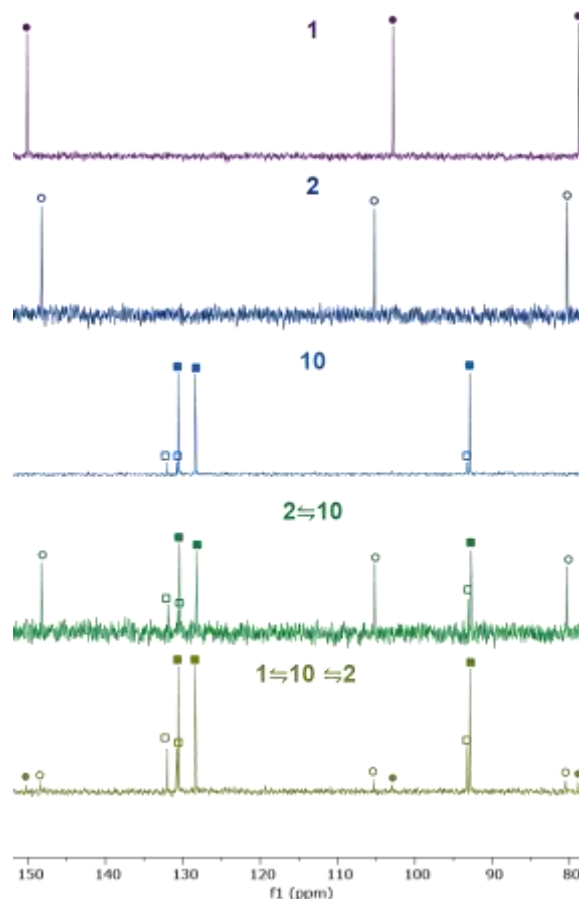

Figure 11. (top to bottom) Detailed region of ^{13}C NMR spectra for **1** (filled circles), **2** (open circles), **10** (squares), and crude reaction mixtures from NiCl₂ mediated isomerization reactions of **2** and **1** showing compounds present in the mixtures.

underpinnings of the differences in reactivity must await further experimentation, including analysis of the intermediate – the allyl oxocarbenium ion.[52] Participation by the C4 or C5 acetate will almost certainly influence the reactivity and stereoselectivity of the reactions of **1** and **2**.[53,54] Glycals exhibiting more VAE react more readily under Ferrier conditions. This rationale is extended to oxepines: **1** reacts more readily than **2** due to the higher prevalence of conformers with a quasi-axial acetate at the allylic center.

A profile of the low energy conformations of **1** and **2** was determined in a tiered process that included an MC conformational search, DFT optimization, and ultimately a least squares regression analysis that utilized $^3J_{H,H}$ coupling constants obtained from ^{1}H NMR spectra. This process was applied in a number of solvents using a CPCM solvation model matched for benzene, chloroform, dichloromethane, acetone, and acetonitrile. For **1**, the most dominant conformer was the $^4H_6$ (63-78%) across all solvents. Additionally, the $^{4,5}TH$ (3-25%) and $^5C_{1,2}$ (7-34%) conformers contributed to the profile of **1**. Analogously, the $^4H_6$ conformation was also the most dominant conformation of **2** (59-71%). Conformers of **2** that were also found were the $^5C_{1,2}$ (29-37%) and the $^6H_4$ (0-6%). While all the conformers observed are part of a broad low-energy surface (0-3 kcal/mol), there is a preference for the $^4H_6$ conformer for both

1 and **2**. In the $^4H_6$ conformation, **1** exhibits a quasi-axial acetoxy group at C3 consistent with the VAE, whereas **2** does not. Additional evidence was sought by attempting to observe the Perlin effect via $^1J_{C,H}$ coupling constants.[55,56] The $^1J_{C,H}$ values for the allylic carbons in **1** and **2** were essentially the same at 152.5 Hz and 149.5 Hz respectively. Similar trends were observed for the C3-OAc bond length of minima DFT conformers (Table S4). When combined with the other conformers in their respective Boltzmann distributions, the consequence is that the %VAE for **1** hovers around 70% for **1** and only 30% for **2**. It is clear that the VAE flows from the preferred conformations of the oxepines rather than being a driver of them. The difference in %VAE of **1** and **2** correlates qualitatively with their reactivities.

Arguments explaining the differential reactivity of oxepine **1** in comparison to **2** in light of their conformational profiles were constructed through the lens of the pyranose system illustrated in Figure 3. There, two C3-epimeric *S*-pyridyl glycals, **6** and **7**, were converted into glycosyl 2,3-anhydro pyranoside **8**. Glycal **7**, which has the same C3 configuration as allal **5**, reacted approximately three times faster than **6**, the analog of glucal, **4**. This example linked high occupancy of a VAE conformer with high reactivity in the Ferrier reaction. We drew a similar correlation with respect to **1** and **2**. Oxepine **1**, with a greater percentage of conformers with a quasi-axial C3 acetoxy group, were decidedly more reactive in the two sets of Ferrier conditions reported. It should be emphasized that this was a correlation and not strictly a causal relationship. We were mindful that oxepine **2** had conformers in its Boltzmann distribution that contained a quasi-axial C3 acetoxy group and that the interconversion of conformers was facile.

A combination of neighboring group participation and the thermodynamic stabilities of the oxepines themselves lend support to the ground state VAE correlation argument. Together, they constitute our rationale for the observed results. The acetoxy group at C4 in oxepine **1** is *anti* relative to the acetoxy group at C3; for **2**, the relationship between them is *syn*. Under the Brønsted or Lewis acidic conditions of the Ferrier rearrangements, the C4 acetoxy group in **1** participates by more readily stabilizing the presumed oxocarbenium ion intermediate. This picture is supported both by intuition and the conformational analysis results where the C3 and C4 acetates are anti-periplanar in the $^4H_6$ conformation of **1**. In terms of thermodynamic stabilities, it is instructive that, in the NiCl$_2$-mediated isomerizations of **1** and **2**, oxepine **2** was observed in the product mixture (along with 2,3-dehydro septanoside **10**) of reactions starting from **1** but the converse was not true. That is, NiCl$_2$-mediated isomerization of **2** gave only **10** and unreacted starting material. We interpret these results as an indication of the ordering of thermodynamic stabilities of these three compounds. So, 2,3-dehydro septanoside **10** is the most stable and **2** is more stable than **1** between the two oxepines. This is consistent with the energies of the active conformations of **1** and **2**. Rearrangement of **1** arises from the $^4H_6$ (1-6) while **2** arises from the $^5C_{1,2}$ (2-92). The difference between the single point energies of both conformers is +0.70 kcal/mol in favor of **2**.

Conclusion

We have utilized computational chemistry and NMR techniques to perform a full-scale conformational analysis of D-glucose and D-mannose-based oxepines **1** and **2**. DFT protocols defined that were previously used only on rigid molecules, translated efficiently to the oxepines investigated. Computed $^3J_{H,H}$ coupling constants, weighted by a MC/DFT Boltzmann distribution of conformers using energies calculated at a B3LYP/6-31G(d,p) level, coincided well with those extracted from ^1H NMR spectra. Better agreement between computed and observed $^3J_{H,H}$ values was achieved when a least squares regression analysis was used. Consistent between both methods was the dominance of the $^4H_6$ half-chair conformation for **1** and **2**. A related half-chair conformation was also adopted in the crystal structure of **3** and suggested that this is the preferred conformation of other substituted seven-membered rings with a rigidifying moiety. The conformational analysis showed that D-glucose based oxepine **1** had a higher %VAE than D-mannose oxepine **2** that correlated with greater reactivity in representative Ferrier rearrangement reactions. This investigation has laid a foundation for additional studies into the oxocarbenium ion intermediate that is presumably common to Ferrier reactions of both **1** and **2** that will be reported in due course.

Author Contributions

C.E.G. executed all the computational, spectroscopic, and synthetic experiments. C.E.G. and M.W.P. contributed to the ideation and preparation of the manuscript.

Conflicts of interest

There are no conflicts to declare.

Acknowledgements

Notes and references

1   M. P. DeMatteo, N. L. Snyder, M. Morton, D. M. Baldisseri, C. M. Hadad and M. W. Peczuh, *J. Org. Chem.*, 2005, **70**, 24–38.

2   M. W. Peczuh and N. L. Snyder, *Tetrahedron Lett.*, 2003, **44**, 4057–4061.

3   V. H. Jadhav, O. P. Bande, R. V. Pinjari, S. P. Gejji, V. G. Puranik and D. D. Dhavale, *J. Org. Chem.*, 2009, **74**, 6486–6494.

4   H. Ovaa, M. A. Leeuwenburgh, H. S. Overkleeft, G. A. Van Der Marel and J. H. Van Boom, *Tetrahedron Lett.*, 1998, **39**, 3025–3028.

5   M. A. Boone, F. E. McDonald, J. Lichter, S. Lutz, R. Cao and K. I. Hardcastle, *Org. Lett.*, 2009, **11**, 851–854.

6   S. Castro, C. S. Johnson, B. Surana and M. W. Peczuh, *Tetrahedron*, 2009, **65**, 7921–7926.

7   N. V. Ganesh, S. Raghothama, R. Sonti and N. Jayaraman, *J. Org. Chem.*, 2009, **75**, 215–218.

8   N. V. Ganesh and N. Jayaraman, *J. Org. Chem.*, 2007, **72**, 5500–5504.

9   C. V. Ramana, A. R. Murali and M. Nagarajan, *J. Org. Chem.*, 1997, **62**, 7694–7703.

10   R. Batchelor and J. O. Hoberg, *Tetrahedron Lett.*, 2003, **44**, 9043–9045.

11   R. Vannam and M. W. Peczuh, *Org. Biomol. Chem.*, 2016, **14**, 3989–3996.

12   C. S. Bennett and M. C. Galan, *Chem. Rev.*, 2018, **118**, 7931–7985.

13   A. Sau and M. C. Galan, *Org. Lett.*, 2017, **19**, 2857–2860.

14   A. Sau, C. Palo-Nieto and M. C. Galan, *J. Org. Chem.*, 2019, **84**, 2415–2424.

15   M. W. Peczuh, N. L. Snyder and W. S. Fyvie, *Carbohydr. Res.*, 2004, **339**, 1163–1171.

16   A. M. Gómez, F. Lobo, C. Uriel and J. C. López, *European J. Org. Chem.*, 2013, **2013**, 7221–7262.

17   F. E. McDonald, A. K. Subba Reddy and Y. Díaz, *J. Am. Chem. Soc.*, 2000, **122**, 4304–4309.

18   D. P. Curran and Y. G. Suh, *Carbohydr. Res.*, 1987, **171**, 161–191.

19   W. R. Roush, D. P. Sebesta and C. E. Bennett, *Tetrahedron*, 1997, **53**, 8825–8836.

20   C. Ernst, M. Piacenza, S. Grimme and W. Klaffke, *Carbohydr. Res.*, 2003, **338**, 231–236.

21   S. Buttar, J. Caine, E. Goné, R. Harris, J. Gillman, R. Atienza, R. Gupta, K. M. Sogi, L. Jain, N. C. Abascal, Y. Levine, L. M. Repka and C. M. Rojas, *J. Org. Chem.*, 2018, **83**, 8054–8080.

22   M. G. Beaver, T. M. Buscagan, O. Lavinda and K. A. Woerpel, *Angew. Chemie Int. Ed.*, 2016, **55**, 1816–1819.

23   F. Groenewald and J. Dillen, *Struct. Chem. 2011 233*, 2011, **23**, 723–732.

24   D. F. Bocian and H. L. Strauss, *J. Am. Chem. Soc.*, 2002, **99**, 2876–2882.

25   K. B. Wiberg, *J. Org. Chem.*, 2003, **68**, 9322–9329.

26   M. P. DeMatteo, S. Mei, R. Fenton, M. Morton, D. M. Baldisseri, C. M. Hadad and M. W. Peczuh, *Carbohydr. Res.*, 2006, **341**, 2927–2945.

27   A. R. Katritzky, N. G. Akhmedov, I. Ghiviriga and R. Maimait, *J. Chem. Soc. Perkin Trans. 2*, 2002, **2**, 1986–1993.

28   S. Dey and N. Jayaraman, *Pure Appl. Chem.*, 2014, **86**, 1401–1419.

29   T. Q. Tran and J. D. Stevens, *Aust. J. Chem.*, 2002, **55**, 171–178.

30   See ESI for additional details on conformer nomenclature.

31   D. Cremer and J. A. Pople, *J. Am. Chem. Soc.*, 2002, **97**, 1354–1358.

32   A. Ardèvol, X. Biarnés, A. Planas and C. Rovira, *J. Am. Chem. Soc.*, 2010, **132**, 16058–16065.

33   A. Nowacki, D. Walczak and B. Liberek, *Carbohydr. Res.*, 2012, **352**, 177–185.

34   The quasi- prefix used throughout the manuscript expresses the nearly-axial or nearly-equatorial disposition of a group on the ring.

35   J. Thiem and P. Ossowski, *J. Carbohydr. Chem.*, 1984, **3**, 287–313.

36   A. Nowacki and B. Liberek, *Carbohydr. Res.*, 2018, **462**, 13–27.

37   K. Takeda, H. Nakamura, A. Ayabe, A. Akiyama, Y. Harigaya and Y. Mizuno, *Tetrahedron Lett.*, 1994, **35**, 125–128.

38   Schrödinger Release 2021-2**:** MacroModel, Schrödinger, LLC, New York, NY, 2021.

39   F. Neese, *Wiley Interdiscip. Rev. Comput. Mol. Sci.*, 2012, **2**, 73–78.

40   F. Neese, *Wiley Interdiscip. Rev. Comput. Mol. Sci.*, 2018, **8**, e1327.

41   All DFT calculations were done in Orca 4.

42   T. Bally and P. R. Rablen, *J. Org. Chem.*, 2011, **76**, 4818–4830.

43   A. Di Salvo, M. David, B. Crousse and D. Bonnet-Delpon, *Adv. Synth. Catal.*, 2006, **348**, 118–124.

44   InabaKiyoshi, MatsumuraShuichi and YoshikawaSadao, *Chem. Lett.*, 1991, **20**, 485–488.

45   Stoddart's protocol begins by positioning the molecule so that the numbering ascends in a clockwise fashion (C1, C2, and so on). The molecule is then rotated until a plane of three or four atoms (i.e, 3=twist chair, 4=chair) is visible. For example, the $^5C_{1,2}$ conformation has a plane containing the C6, O, C3, and C4, with C6 and the O in the front and C3 and C4 in the rear. When observing this conformation through the plane it is apparent that the C5 is above the molecular plane (superscript) and C1 and C2 are below it (subscript).

46   K. Bock and J. Ø. Duus, *J. Carbohydr. Chem.*, 2006, **13**, 513–543.

47   E. Juaristi and S. Antúnez, *Tetrahedron*, 1992, **48**, 5941–5950.

48   E. L. Eliel and S. H. Wilen, *Stereochemistry of Organic Compounds*, Wiley-Interscience, Hoboken, NJ, USA, 1st edn., 1994.

49   There was one exception, a conformer of **1** (1-276), that contained and *E* configured ester at the C5 position. (Fig. S1D) Because this conformer did not contribute to the Boltzmann distribution for **1**, it was not further investigated.

50   T. Turney, Q. Pan, L. Sernau, I. Carmichael, W. Zhang, X. Wang, R. J. Woods and A. S. Serianni, *J. Phys. Chem. B*, 2016, **121**, 66–77.

51   Heating a solution of a tri-*O*-acetyl-D-glycal in acetic anhydride at 120 °C with a stoichiometric amount of nickel(II) chloride will produce a mixture of C3 epimers and 1,4,6-tri-*O*-acetyl-D-erythro-hex-2-enopyranose.

52   N. Bhuma, L. Lebedel, H. Yamashita, Y. Shimizu, Z. Abada, A. Ardá, J. Désiré, B. Michelet, A. Martin-Mingot, A. Abou-Hassan, M. Takumi, J. Marrot, J. Jiménez-Barbero, A. Nagaki, Y. Blériot and S. Thibaudeau, *Angew. Chemie Int. Ed.*, 2021, **60**, 2036–2041.

53   M. Marianski, E. Mucha, K. Greis, S. Moon, A. Pardo, C. Kirschbaum, D. A. Thomas, G. Meijer, G. von Helden, K. Gilmore, P. H. Seeberger and K. Pagel, *Angew. Chemie Int.*

Ed., 2020, **59**, 6166–6171.

54   K. Greis, C. Kirschbaum, S. Leichnitz, S. Gewinner, W. Schöllkopf, G. von Helden, G. Meijer, P. H. Seeberger and K. Pagel, *Org. Lett.*, 2020, **22**, 8916–8919.

55   S. Wolfe, B. M. Pinto, V. Varma and R. Y. N. Leung, *Can. J. Chem.*, 1990, **68**, 1051–1062.

56   A. S. Perlin and B. Casu, *Tetrahedron Lett.*, 1969, **10**, 2921–2924.